Studies on Solute−Solvent Interactions in Gaseous and Supercritical Carbon Dioxide by High-Pressure 1H NMR Spectroscopy

ARTICLE *in* THE JOURNAL OF PHYSICAL CHEMISTRY B · MARCH 2000

Impact Factor: 3.3 · DOI: 10.1021/jp992278n

7 AUTHORS, INCLUDING:

Takanori Kawakami
Hokkaido University
20 PUBLICATIONS **160** CITATIONS

SEE PROFILE

Norio Saito
National Cancer Center, Japan
172 PUBLICATIONS **2,759** CITATIONS

SEE PROFILE

高圧 ^{1}H NMR分光法による気体および超臨界二酸化炭素中の溶質－溶媒相互作用に関する研究*1

金久保光央*2、相沢崇史*2、川上貴教*2、佐藤　修*2、生島　豊*2、畑田清隆*2、斎藤功夫*3

Studies on Solute-Solvent Interactions in Gaseous and Supercritical Carbon Dioxide by High-Pressure ^{1}H NMR Spectroscopy

M. Kanakubo, T. Aizawa, T. Kawakami, O. Sato, Y. Ikushima, K. Hatakeda, N. Saito

A newly designed high-pressure NMR flow cell has been developed for studies of supercritical fluids. By using the high-pressure cell, ^{1}H chemical shifts of nonpolar (*n*-hexane and benzene) and polar (dichloromethane, chloroform, acetonitrile, water, methanol, and ethanol) solute molecules in gaseous and supercritical carbon dioxide were measured in the wide pressure range between 2 and 30 MPa at 313.3 K. The chemical shifts of hydroxyl protons of water, methanol, and ethanol in carbon dioxide at 20.0 MPa were shifted to higher frequency due to intermolecular hydrogen bonding with increasing concentration. A comparison of the concentration dependence with relevant data in carbon tetrachloride indicated a specific interaction between alcohol and carbon dioxide molecules. The corrected ^{1}H chemical shifts of nonpolar and polar solute molecules at infinite dilution, where the bulk magnetic susceptibility contribution was subtracted, were shifted to higher frequency with increasing density of carbon dioxide. The observed density dependence, represented by a polynomial equation of the third power of density, was interpreted in terms of three distinct density regions, i.e., *gaslike*, *intermediate*, and *liquidlike*. In the gaslike and liquidlike states the solvation structure rapidly varies as the bulk density increases, whereas in the intermediate state the solvation structure remains almost unchanged despite the drastic change in the bulk density. It was demonstrated that the ^{1}H chemical shift is quite a sensitive probe to a variation of surroundings. The solvent-induced ^{1}H chemical shifts were analyzed on the basis of two different models.

Introduction

Supercritical carbon dioxide, sc-CO_2, is one of the most attractive media from not only scientific but also industrial viewpoints because CO_2 is environmentally acceptable, nonflammable, relatively nontoxic, and inexpensive, and the solvent properties of sc-CO_2 can be tuned widely by adjusting pressure and temperature. In the past decade many workers[1] have vigorously investigated chemical and biochemical reactions in sc-CO_2: it was observed that the reaction rates increased near the critical point (304.2 K and 7.38 MPa),[2] which was attributable to specific solute−solvent and solute−solute interactions. In addition to the reaction studies, solute−solvent interactions in sc-CO_2 have been investigated as well by means of UV and vibrational spectroscopies.[3] For example, with FT-IR spectroscopy Fulton et al.[4] examined the degree of intermolecular hydrogen bonding between solute molecules of methanol-*d* in sc-CO_2, sc-ethane, and liquid heptane, and suggested a formation of some type of weak complex between CO_2 and methanol molecules.

sc-CO_2 is an entirely nonpolar solvent, and the solvent properties are represented by a low permittivity, a low Hildebrand solubility parameter, and a low polarizability of the molecule. On the other hand, a CO_2 molecule has a large quadrupole moment, and electron donor and acceptor sites. Therefore, when a nonpolar or polar solute molecule without an electric charge is introduced into sc-CO_2, solute−solvent interactions are limited to van der Waals dispersion interaction for a nonpolar solute or van der Waals and polar (dipole−induced dipole and dipole−quadrupole) interactions for a polar solute. UV and vibrational spectroscopies, as mentioned above, are surely powerful tools for investigation of such weak interactions directly or indirectly. An NMR spectroscopy has frequently been used for studies on solute−solvent interactions in solution,[5] and its chemical shift of protons located at a peripheral surface of a molecule should be one of the most sensitive probes. Advantageously it has a wide application to any NMR active nuclei, and its relaxation rate is closely related to translational and rotational motions of molecules. The measurements are favorably less affected by critical opalescence. It is further stressed that reliable pictures of solute−solvent interactions in sc-CO_2 should be derived on the basis of various experimental techniques. Until now, however, only a few studies[6−9] on NMR chemical shifts have been performed in sc-CO_2 because several experimental difficulties under high magnetic field have to be overcome for the precise measurements of chemical shifts in the supercritical state.

A high-resolution and high-pressure NMR instrument has been well established as reported previously.[10,11] However, the samples employed were gases or liquids, the densities of which are relatively insensitive to temperature. For the measurements in supercritical fluids, it is of great importance to stabilize a sample temperature in a large portion of the system because the density near the critical point changes drastically with temperature, which readily results in convection flow in nonviscous supercritical fluids. One of the best designs for the high-pressure NMR cell for supercritical fluids, as reported by Pfund et al.,[12] is a capillary vessel made of a fused silica. Their unique high-pressure tubing is safe from breaks and inexpensive,

*1 This paper was reprinted from The Journal of Physical Cemistry B, Vol.104, No.12, pp.2749-2758, with permission of American Chemical Society.

*2 Chemical-Reaction Science Section
*3 Inorganic Materials Section

but may be easily damaged and has a very small volume of sample, which makes experiments of low sensitive nuclei difficult. We herein present a newly designed high-pressure NMR flow cell for supercritical fluids: (i) the inhomogeneity of the sample temperature can be reduced as small as possible, (ii) it is mechanically heavy-duty, (iii) it has a relatively large volume of sample, (iv) it is usable in every commercial NMR spectrometer with a narrow bore, (v) a sample concentration is determined with an in situ measurement, and (vi) the contribution of magnetic susceptibility can be corrected for quantitatively. With the present flow cell, moreover, one may pursue reaction pathways in supercritical fluids such as a recent topic of organometallic reactions.[13]

In the present study, by using the high-pressure NMR cell, we measure ^1H chemical shifts of nonpolar (*n*-hexane and benzene) and polar (dichloromethane, chloroform, acetonitrile, water, methanol, and ethanol) solute molecules in gaseous and supercritical CO_2 in the wide pressure range between 2 and 30 MPa at 313.3 K. The ^1H chemical shift reported here provides some important insights into the variation of the surroundings of the solute molecule with the density of CO_2.

Experimental Section

High-Pressure NMR Flow Cell. It has been reported that high-pressure cells for NMR measurements were made of nonmagnetic plastic,[14] sapphire,[11] and fused silica.[12] The cell used in our work was fabricated from mechanically strong and also nonmagnetic ceramic material. Previously we reported that ^1H NMR spectra in sc-CO_2 were successfully measured with a batch type of ceramic cell.[15] In the present study, a newly designed flow type of the cell was established with several important improvements as follows. A schematic drawing of the cell is given in Figure 1. A ceramic tube (j) manufactured by Kyocera Corp. had a 10 mm outer diameter, a 5 mm inner diameter, and a 170 mm length. To the top of the ceramic tube (j) high-pressure valves (b and c) were attached, which were constructed from nonmagnetic Ti−Al alloy. The ceramic tube was inserted into the Ti−Al valve seat (c) and fixed with a Teflon ring (h). Then, the valve stem (b) and seat (c) were connected by seven threads with a 10 mm Teflon cushion (g) and Hyker O-ring (f) between the stem and seat. Another Hyker O-ring (f) put in a groove of the valve stem worked as a movable seal between the valve stem and the inner surface of the seat. The valve stem had three 1/16 in. diameter holes drilled through. Standard 1/16 in. Swagelok fittings (a) were usable for the top threaded sections in the valve stem, which were connected to the three holes, respectively. These three ports were used for an inlet and outlet of sample solutions, and for a thermocouple (d) to monitor sample temperatures directly. To transport sample solutions directly to the observed region of the rf coil, a 1/16 in. Ti tube (i) was inserted into the high-pressure cell, the bottom end of which was located at a position 30 mm from the rf coil. This alignment can bring about a favorable solution flow in the high-pressure cell: the sample solution in the rf region supplied through the Ti tube passes away toward the outlet (e) at the top of the cell along the inner wall. A 1/16 in. stainless 316 outlet tube (e) was connected to an external back-pressure regulator. No pressure difference between the inlet and outlet in the cell had been checked preliminarily. The present NMR cell can stand, at least, high pressures up to 30 MPa and temperatures up to 393 K. The simple and mechanically strong design of the cell allows safe use in every commercial NMR probe without an expensive modification of the probe. This high-pressure flow cell cannot be rotated, but the recent progress in superconducting magnets enables us to measure high-resolution spectra without rotating the sample.

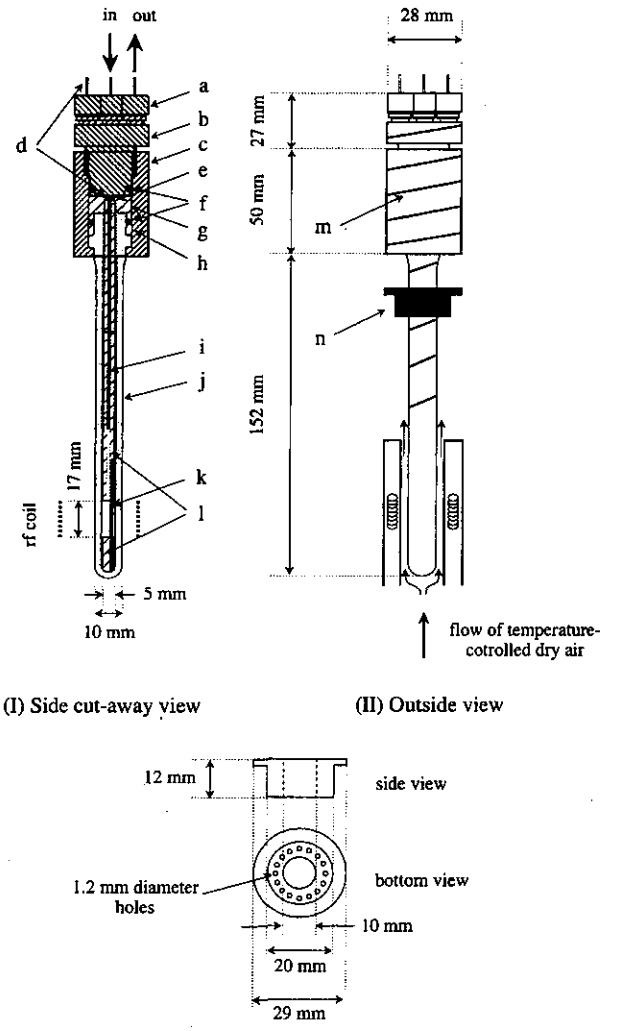

Figure 1. High-pressure on-line NMR cell. (I) Side cut-away view: (a) 1/16 in. Swagelok fittings, (b) Ti−Al valve stem, (c) Ti−Al valve seat, (d) thermocouple, (e) 1/16 in. stainless steel outlet tube, (f) Hyker O-rings, (g) Teflon cushion, (h) Teflon ring, (i) 1/16 in. Ti inlet tube, (j) ceramic tube, (k) TMS−C_6D_6 reference, and (l) Teflon spacers. (II) Outside view: (m) manganin wire for heating and (n) sample holder (see also Figure 2 (III)). (III) Air-through type of sample holder.

The temperature was controlled by a heated dry gas with a temperature controller unit of the spectrometer. The heated dry gas flowed up from the bottom of the sample cell (Figure 1 (II)). The temperature at the upper portion of the sample cell unpleasantly deviated down: the temperature difference from the bottom of the cell went up to approximately −6 K under the control of the dry gas at 313.3 K. To reduce the temperature deviation, we made several improvements in the high-pressure cell. (i) A sample holder (usually used for rotating a sample tube) was newly designed as an air-through type (Figure 1 (III)). (ii) The temperature at the upper portion of the high-pressure cell was adjusted by an additional heater. A polyester-coated manganin wire of 0.1 mm diameter (m) wound around the cell (resistance ~84 Ω) was controlled by an external dc power supply on measuring the sample temperature directly with a Cu−constantan thermocouple (d) that was inserted into the cell. The heater at a distance of 20 mm from the rf coil led to no rf

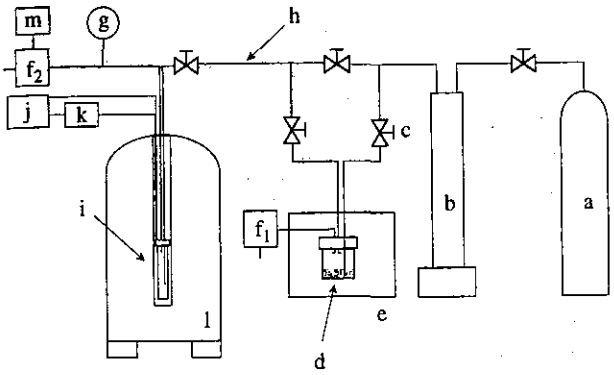

Figure 2. Schematic diagram of the high-pressure apparatus used for the on-line NMR spectroscopy: (a) CO_2 cylinder, (b) syringe pump, (c) high-pressure valve, (d) mixing vessel for preparing the solutions, (e) oven, (f) back-pressure regulator with digital pressure gauge, (g) Bourdon pressure gauge, (h) insulation jacket, (i) high-pressure cell, (j) dc power supply, (k) indicator of the thermocouple, (l) superconducting magnet, and (m) recorder.

noise, no additional magnetic field, and no trouble in shimming adjustments without any radiation shield. Owing to the two improvements, the sample temperature was kept constant within ±0.2 K over the sample cell. In addition to minimizing the temperature inhomogeneity, the heater advantageously made the solution flow smooth; i.e., it prevented dissolved solutes from being condensed at the upper portion of the cell. (iii) The useless space in the high-pressure cell was filled with Teflon spacers (l), and the sample solution was positioned only at the portion observed by the rf coil. The effective sample volume was relatively large (~0.3 cm^3), which made experiments under extremely dilute conditions easier. These Teflon spacers were conveniently used as the well for standing a capillary tube (k) containing a TMS−C_6D_6 solution parallel to the externally applied magnetic field.

Sample Preparations at High Pressures. A schematic diagram of the high-pressure apparatus in the present system is shown in Figure 2. CO_2 supplied from a cylinder (a) was pressurized with an Isco syringe pump (b), model 260D. The high-pressure cell and line were purged with approximately 5 MPa of CO_2 gas before each run of experiments. An excess amount of liquid solute was in advance introduced into a mixing vessel (d) consisting of a 30 cm^3 stainless 316 container. The solute liquid was degassed by passing through the solvent gas several times. The impure gas containing air was removed from the system through the back-pressure regulator (f_1) connected to the mixing vessel. The mixing vessel was heated at 318 K by an oven (e). The mixture was stirred with a magnetic stir bar, and then the CO_2 solution of the upper phase in the vessel was transferred into the high-pressure cell through a 1/16 in. stainless 316 tube covered with a thermal insulation jacket (h). It took about 30 min to flush the high-pressure cell and line for preparing different samples of unique solutes. The sample concentration was adjusted by introducing pure CO_2 carefully through a bypass line. Once the sample was prepared in the NMR cell, the high-pressure valve above a superconducting magnet (l) was closed. The system was allowed to equilibrate for, at least, 30 min between 7 and 11 MPa and for 20 min at other pressures. Pressures were increased stepwise from 2 to 30 MPa in each run of experiments. The pressure of the sample solution was measured with a pressure gauge built in a back-pressure regulator (f_2), JASCO 880-81, which was connected to the outlet in the high-pressure cell. The pressures measured with the pressure gauge showed values identical with those of a Bourdon pressure gauge (g). A pressure fluctuation during the measurements was output to a recorder (m), and the uncertainty was estimated to be ±0.05 MPa at most.

NMR Experiments. High-resolution ^1H NMR spectra were obtained using a Varian Inova 500 spectrometer equipped with a standard 10 mm probe. The proton resonance frequency was 499.87 MHz. A standard single pulse sequence of 12 μs (ca. a 45° pulse width) was used for all experiments. The repetition time was longer than 5 times the longitudinal relaxation time ($>5T_1$). The number of scan times was 1−8, depending on the signal sensitivity. The spectral width was fixed to be 8000 Hz, and the digital resolution was higher than 0.24 Hz. A reference solution of 1% v/v or less TMS-C_6D_6 was sealed into an approximately 1.5 mm diameter Pyrex capillary tube. Deuterated benzene in the capillary tube was used as an external lock solvent and for a shim coil adjustment. The resolution of the spectra was ascertained to be higher than 5 Hz in the pressure range between 9 and 30 MPa. A relatively low resolution (<10 Hz) at low pressures was due to a failure of the shimming adjustments: magnetic field inhomogeneity still remained because of quite different magnetic susceptibilities between gaseous samples and Teflon spacers. Over the pressure-variable experiment, no change in the rf tuning and pulse width was observed.

The sample concentration was quantitatively determined from the relative peak area of the solute protons to that of the TMS protons. A calibration had been made preliminarily at the same temperature of the experiments: the proton concentration was proportional to the relative peak area within ±2% uncertainty. The appropriate capillary reference was chosen to correspond to the sample concentration in each measurement.

Bulk Magnetic Susceptibility Corrections. ^1H chemical shifts of various solutes in CO_2 at a fixed temperature of 313.3 K were recorded with the TMS signal as an external reference. This external reference method, which can eliminate the medium effects on the shielding constant of the reference, by itself, is desirable because a relatively inert TMS signal should be affected by a change in surroundings as reported previously.[16,17] The capillary reference tube was fixed at an ideal geometry with Teflon spacers, i.e., parallel to the externally applied magnetic field. An exchange of capillary tubes caused no serious error in the chemical shifts, which enabled us to make a reproducible correction for the bulk magnetic susceptibility.

The observed chemical shift, δ_{obs}, was referenced with respect to the TMS signal at 298.2 K. The bulk magnetic susceptibility correction was made by (cgs emu unit)[18,19]

$$\delta_{corr} = \delta_{obs} + \frac{4\pi}{3}\{\chi(\mathrm{ref}) - \chi(\mathrm{sam})\} \times 10^6 \qquad (1)$$

where δ_{corr} is the susceptibility-corrected chemical shift and χ(ref) and χ(sam) are the volume magnetic susceptibilities of the reference and sample solutions, respectively.

The χ(ref) of the reference solution in the capillary tube at 313.3 K was estimated to be a constant of -0.630×10^{-6} by the following procedure. χ of C_6D_6 was first determined to be -0.630×10^{-6} at 298.2 K by measuring the signal separation of TMS between C_6H_6 and C_6D_6 solutions, where a value of -0.622×10^{-6} was used for χ of C_6H_6.[20] The temperature variation of χ(ref) was evaluated from that of δ of the TMS signal; however, it held no significance. In the above calculations, we assumed that the change in δ of TMS was attributable to that in χ.

On the other hand, χ(sam) of CO_2 solutions could be calculated by the following equation if the infinitely dilute

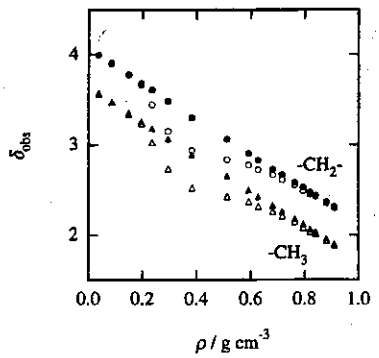

Figure 3. Density dependence of δ^{∞}_{corr} of *n*-hexane in carbon dioxide at 313.3 K. The triangles and circles represent the CH_3 and CH_2 signals, respectively. The closed and open symbols indicate the different experimental conditions with and without the top heater and Teflon spacers, respectively. See the text.

condition was satisfied:

$$\chi(\text{sam}) \approx \chi(CO_2) = \frac{\rho}{M}\chi_m(CO_2) \qquad (2)$$

Here, $\chi_m(CO_2)$ is the molar magnetic susceptibility of CO_2 (=-20.8×10^{-6} cm^3 mol^{-1}),[21] M is the molar mass of CO_2, and ρ is the density of CO_2, which can be interpolated according to the standard procedure.[2] In the present study, χ(sam) was assumed to be the same as $\chi(CO_2)$ because the experiments were performed under sufficiently dilute conditions: the concentrations, c, of solutes in CO_2 were prepared up to, at most, 250 mol m^{-3}. In fact, no concentration dependence of the chemical shifts of *n*-hexane, benzene, dichloromethane, chloroform, and acetonitrile in CO_2 was observed at any pressure: the chemical shifts measured at $c < 5$ mol m^{-3} ($\rho \leq 0.25$ g cm^{-3}) and at $c < 10$ mol m^{-3} (0.25 g cm^{-3} < ρ) could be regarded as the chemical shifts at infinite dilution. The chemical shifts of hydroxyl protons of water, methanol, and ethanol in CO_2 at constant pressures apparently increased with increasing c, whereas the chemical shifts of the CH_3 and CH_2 (only of ethanol) protons of methanol and ethanol remained virtually unchanged within the experimental errors. The latter invariance certainly proved that eq 2 could hold. The infinitely dilute values of the chemical shifts of water, methanol, and ethanol were estimated under sufficiently dilute conditions of $c < 1$ mol m^3 ($\rho \leq 0.25$ g cm^{-3}), $c < 3$ mol m^3 (0.25 g cm^{-3} < $\rho \leq 0.65$ g cm^{-3}), and $c < 5$ mol m^3 (0.65 g cm^{-3} < ρ) in view of their concentration dependence.

Chemicals. Reagent-grade *n*-hexane and benzene and HPLC-grade dichloromethane were purchased from Nacalai Tesque, Inc. Spectroscopic-grade acetonitrile and chloroform were obtained from Dojindo Laboratories. Dehydrated methanol and ethanol were purchased from Wako Pure Chemical Industries, Ltd., and purified water was purchased from Sanchemifa K. K. Pure-grade carbon dioxide from Sumitomo Seika Chemicals Co., Ltd. was 99.9% in purity. All chemicals were used without further purification.

Results and Discussion

Verification of the High-Pressure Cell. The observed chemical shifts, δ^{∞}_{obs}, of *n*-hexane in CO_2 at infinite dilution and at 313.3 K are plotted against the density of CO_2, ρ, in Figure 3 (closed symbols), where the triangle and circle denote the CH_3 and CH_2 protons, respectively. The coupling constant, $^3J_{HH}$, observed in the CH_3 signal remains a usual value of 6–7 Hz over the density range. We also plot the data (open symbols) in Figure 3 by using the high-pressure cell without the top heater and Teflon spacers. As seen in Figure 3, an unexpected deviation at 0.2 g cm^{-3} < ρ < 0.65 g cm^{-3}, corresponding to the region of large compressibilities of CO_2, is observed in the absence of the cell improvements. Since no intermolecular interaction bringing about a low-frequency shift is considered in the present case, the large deviation is attributable to an unsuccessful experimental setup, i.e., to a convection flow caused by inhomogeneous sample temperature. With our developed high-pressure cell, on the other hand, δ^{∞}_{obs} almost linearly decreases with a raise of ρ for either the CH_3 or CH_2 protons. The reproducibility of δ^{∞}_{obs} is within ±0.02 at 0.2 g cm^{-3} < ρ < 0.65 g cm^{-3} and within ±0.01 at the other densities. The slopes for the CH_3 and CH_2 protons are -1.94 ± 0.03 and -1.97 ± 0.04 cm^3 g^{-1}, corresponding to -85.4 ± 1.2 and -86.8 ± 1.8 cm^3 mol^{-1}, respectively, in the range of ρ < 0.4 g cm^{-3}, where the uncertainties are given by the 95% confidence limit. A slight high-frequency shift at higher densities is caused by van der Waals interaction as discussed later. These results are slightly smaller than the reported values of -1.84 and -1.87 cm^3 g^{-1} for the CH_3 and CH_2 protons of *n*-hexane in CO_2, respectively.[9] This difference can be attributable to the density range used for the determination: Dardin et al.[9] employed the chemical shift data over the density range between 0.2 and 0.9 g cm^{-3}. The change in δ^{∞}_{obs} with ρ arising from the bulk magnetic susceptibility change can be expressed as $(4\pi/3M)\chi_m(CO_2) \times 10^6$, which gives -1.98 cm^3 g^{-1}. The slope for the inner-positioned CH_2 protons, with which solvent CO_2 molecules may be less interactive, shows fairly good agreement with the magnetic susceptibility contribution. This fact indicates that our developed high-pressure cell works well over the gaseous-to-supercritical states.

Concentration Dependence of Chemical Shifts of Hydroxyl Protons. The corrected chemical shifts, δ_{corr}, of hydroxyl protons of water, methanol, and ethanol in CO_2 at 20.0 MPa and at 313.3 K were apparently shifted to higher frequency with increasing c (Figure 4a). The relevant δ_{corr} values of hydroxyl protons of methanol and ethanol in carbon tetrachloride measured at atmospheric pressure and at the same temperature are plotted as well in Figure 4b: note that the range of the vertical axis scaled is twice that in Figure 4a. The relation between δ_{corr} and c for methanol and ethanol in CO_2 and carbon tetrachloride is well expressed by a quadratic equation:

$$\delta_{corr}(c) = k_0 + k_1 c + k_2 c^2 \qquad (3)$$

where the coefficients are determined by the least-squares secondary regression (Table 1). However, the third term in eq 3 is negligibly small for δ_{corr} of water in the range of $c < 100$ mol m^{-3}, and δ_{corr} is linearly related to c.

A similar concentration dependence of chemical shifts of hydroxyl protons has been observed in several organic solvents.[22–24] It has generally been interpreted in terms of a change in successive equilibria with a series of hydrogen-bonded species. According to Gutowsky and Saika,[25] the time-averaged chemical shift of hydroxyl protons, as the lifetime of hydrogen-bonded species is much shorter than the NMR time scale, was given by a weighted average of the chemical shifts of free and hydrogen-bonded species. Thus

$$\delta_{corr}(c) = \frac{c_1}{c}\delta_{free} + \frac{c_2}{c}\delta_{dimer} + \frac{c_3}{c}\delta_{trimer} + \cdots \qquad (4)$$

Here, c is the total concentration, c_1 and δ_{free} are the concentra-

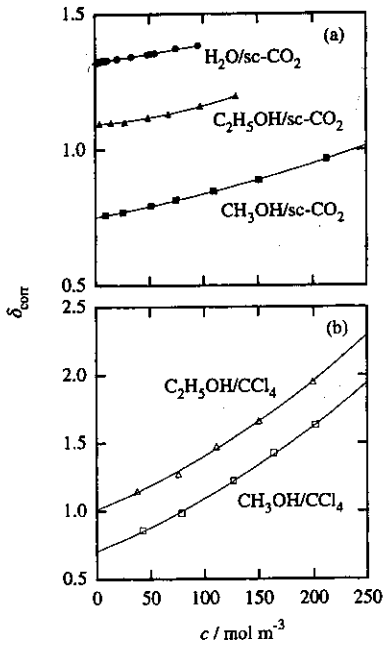

Figure 4. Concentration dependence of δ_{corr} of hydroxyl protons of water (circles), methanol (squares), and ethanol (triangles) in carbon dioxide at 20.0 MPa (a) and in carbon tetrachloride (b) at 313.3 K. The lines represent the quadratic regressed fits of the data for methanol and ethanol, and the linearly regressed fit of the data for water. Note that the range of the vertical axis scaled in (b) is twice that in (a).

tion and the chemical shift of free molecules, c_2, c_3, ... are the concentrations belonging to the dimer, trimer, ..., and δ_{dimer}, δ_{trimer}, ... refer to the corresponding chemical shifts, respectively. Since the formation of hydrogen bonds commonly causes a high-frequency shift, the observed concentration dependence clearly indicates the presence of hydrogen-bonded species even at such dilute concentrations, $c < 250$ mol m^{-3}. Equation 4 predicts an upward deviation from linearity with increasing c (the third term in eq 3), which originates from displacements of the successive equilibria to higher-order hydrogen-bonded species. The linear relationship for water probably suggests the absence of higher-order hydrogen-bonded species at $c < 100$ mol m^{-3}.

For further analyses we assume that the solute molecules belong to two extreme states, either the "free" or the "n-mer" state. The free solute molecule is surrounded entirely by solvent molecules without solute–solute interactions: its chemical shift, δ_{free}, is given by the k_0 value in each solvent. The n-mer solute molecule, in contrast, is a member of the highest-order hydrogen-bonded species in solution: the chemical shift of the n-mer solute molecule, δ_{n-mer}, is assumed to be the same as that of pure liquid consisting of the solute molecules alone, δ_{liq} (Table 1). The two-state model is certainly an oversimplification and is not rigorous. Nevertheless, this simplified model is very practical for analyses of the chemical shifts, and the inferences will provide meaningful information on the average state of hydrogen-bonded species. In fact, on the basis of this model Hoffmann and Conradi[26] have discussed the extent of hydrogen bonding in supercritical water and alcohols. The two-state model gives the fraction of free solute molecules, c_1/c:

$$\frac{c_1}{c} = \frac{\delta_{corr}(c) - \delta_{n-mer}}{\delta_{free} - \delta_{n-mer}} \approx \frac{\delta_{corr}(c) - \delta_{liq}}{k_0 - \delta_{liq}} \qquad (5)$$

The c_1/c value thus obtained is plotted against the mole fraction of the solute, x_{solute}, in Figure 5. The straight line drawn diagonally from $c_1/c = 1$ at $x_{solute} = 0$ to $c_1/c = 0$ at $x_{solute} = 1$ indicates a linear decrement of c_1/c with x_{solute}.

Figure 5 provides very important features about solute–solute and solute–solvent interactions in solutions as follows. (i) All the data points apparently fall below the straight line, which is again clear evidence of aggregation due to intermolecular hydrogen bonding. (ii) The extent of downward deviation in carbon tetrachloride is much greater, by a factor of about 2.2 in the range of $x_{solute} \leq 0.01$, than that in CO_2 for methanol and ethanol. This means that the solvent CO_2 molecules prevent promotion of hydrogen-bonded species. In view of the neutral nature of the two solvent molecules, this fact strongly suggests a specific interaction between alcohol and CO_2 molecules. This observation is in good agreement with the results for methanol-d of Fulton et al.[4] by means of FT-IR spectroscopy; however, a direct comparison cannot be made because their measurements were carried out mainly at higher concentrations ($0.01 < x_{solute}$). (iii) The data points appear to converge on a single curve in each solvent. In CO_2 solutions, however, a slight difference is observed (see the inset of Figure 5): the fractions of free molecules for water and methanol are faintly less than that for ethanol. Certainly this difference will reflect the effect of the alkyl chain as discussed elsewhere.[15] Anyway, we conclude that the equilibria of hydrogen-bonded species are predominantly determined by solute–solvent interactions.

Density Dependence of Chemical Shifts at Infinite Dilution. The corrected chemical shifts, δ^{∞}_{corr}, of a variety of solutes in CO_2 at infinite dilution and at 313.3 K are plotted against the density of CO_2, ρ, in Figures 6–8. They show a unique density dependence. Here we can divide the density dependence into three regions, *gaslike*, *intermediate*, and *liquidlike*. The δ^{∞}_{corr} increases linearly with an increase of ρ up to, at least, 0.2 g cm^{-3} (gaslike), then is less sensitive to ρ between 0.3 and 0.6 g cm^{-3} (intermediate), and further increases with ρ at higher densities, 0.6 g cm^{-3} < ρ (liquidlike). Over the observed density range, the variation of δ^{∞}_{corr} is well represented by the polynomial equation of the third power of ρ:

$$\delta^{\infty}_{corr}(\rho) = \delta_0 + \delta_1\rho + \delta_2\rho^2 + \delta_3\rho^3 \qquad (6)$$

where δ_0 corresponds to the chemical shift of an isolated solute molecule. The coefficients are obtained by using a least-squares program with 95% confidence limits (Table 2). A similar virial expansion has frequently been used to express the density dependence of the shielding constant for a gaseous sample at a fixed temperature:[27–29] the shielding constant, σ, is related to the chemical shift by definition, $\delta = (\sigma_r - \sigma)/(1 - \sigma_r) \times 10^6 \approx (\sigma_r - \sigma) \times 10^6$, where σ_r is the shielding constant of the reference substance.

An explicit expression for a solvent-induced chemical shift can be given by using a radial distribution function, $g(r)$, on the assumption that only pairwise interactions are the predominant factors:[12,30]

$$\delta^{\infty}_{corr} - \delta_0 = -10^6(\sigma - \sigma_0) = -10^6\sum_i\langle\sigma_i\rangle = -10^6\sum_i\left\{N_A\frac{\rho}{M}\int\sigma_i(r)\,g(r)\,4\pi r^2\,dr\right\} \qquad (7)$$

where σ_0 is the shielding constant of an isolated solute molecule, N_A is Avogadro's constant, and the angular brackets refer to the total contribution over the system. In eq 7 the shielding constant arising from solute–solvent interactions is considered

TABLE 1: Values of k_0, k_1, and k_2 for δ_{corr} of Hydroxyl Protons for Water, Methanol, and Ethanol in Carbon Dioxide at 20.0 MPa and in Carbon Tetrachloride at 313.3 K, and δ_{liq} of Hydroxyl Protons for the Corresponding Pure Liquids at 313.3 K[a]

solute	solvent	k_0	$k_1/10^{-2}$ m^3 mol^{-1}	$k_2/10^{-4}$ m^6 mol^{-2}	δ_{liq}[b]
water	sc-CO_2	1.289(2)	0.063(4)		5.008
methanol	sc-CO_2	0.720(6)	0.074(13)	0.013(6)	4.999
	CCl_4	0.673(130)	0.312(243)	0.074(99)	
ethanol	sc-CO_2	1.061(6)	0.029(21)	0.039(15)	5.538
	CCl_4	0.980(175)	0.312(336)	0.081(139)	

[a] The 95% confidence limit in the least significant digits is given in parentheses. [b] The bulk magnetic susceptibility correction has been made.

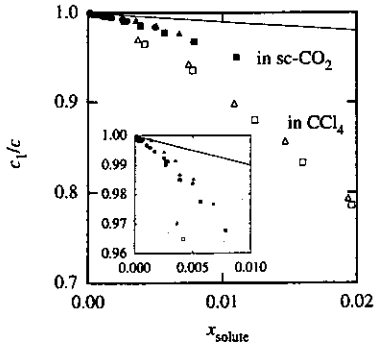

Figure 5. c_1/c vs x_{solute} for water (circles), methanol (squares), and ethanol (triangles) in carbon dioxide at 20.0 MPa (closed symbols) and in carbon tetrachloride (open symbols) at 313.3 K. The upper left region is expanded as an inset. The straight line is drawn diagonally from $c_1/c = 1$ at $x_{solute} = 0$ to $c_1/c = 0$ at $x_{solute} = 1$.

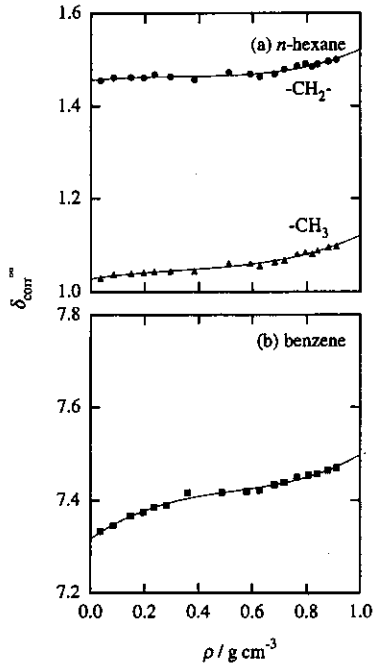

Figure 6. Density dependence of δ^{∞}_{corr} of *n*-hexane (a) and benzene (b) in carbon dioxide at 313.3 K. The lines represent the third-order regressed fits of the data.

to be split into several independent terms:[20,31]

$$\sum_i \langle \sigma_i \rangle = \langle \sigma_a \rangle + \langle \sigma_W \rangle + \langle \sigma_e \rangle \qquad (8)$$

Here, σ_a is the contribution from magnetic anisotropy of the solvent molecule, σ_W is the contribution from van der Waals dispersion interaction, and σ_e is the polar effect, i.e., the contribution from permanent electric interactions between solute and solvent molecules. In accordance with the previous studies,[7,11] we assume that σ_a is negligible for a CO_2 molecule. Since σ_W and σ_e are expected to be negative, bringing about high-frequency shifts, and are inversely proportional to the intermolecular distance, r, to the sixth or fourth power, as discussed later, δ^{∞}_{corr} should be a sensitive measure of solvation structure around the solute protons. Although a similar density dependence has been observed for various spectroscopic shifts of probe molecules that are sensitive to the local solvent environment,[32] this is the first, to our knowledge, to clarify the density dependence of the solvent-induced NMR chemical shift of the solute molecule over the gaseous-to-supercritical densities.

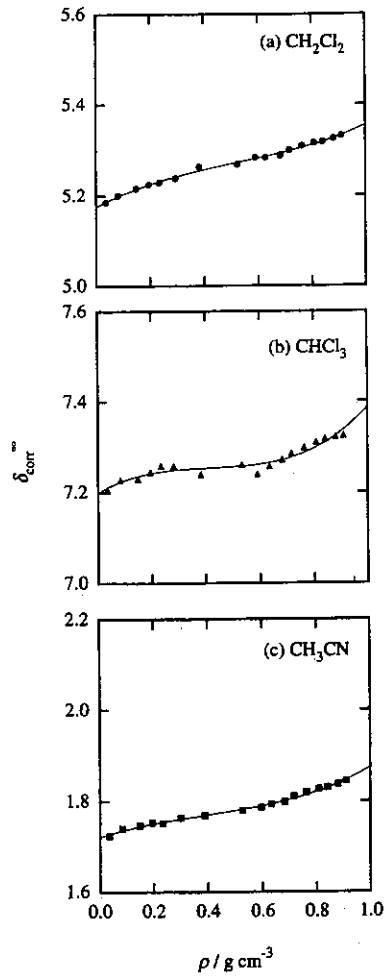

Figure 7. Density dependence of δ^{∞}_{corr} of dichloromethane (a), chloroform (b), and acetonitrile (c) in carbon dioxide at 313.3 K. The lines represent the third-order regressed fits of the data.

The structure of the solvation sphere around the solute molecule in CO_2 can be discussed in terms of the above-mentioned three distinct density regions. In the gaslike and liquidlike states, obviously, the structure of the solvation sphere rapidly varies with increasing bulk density ρ, whereas in the intermediate state the solvation structure is almost retained in

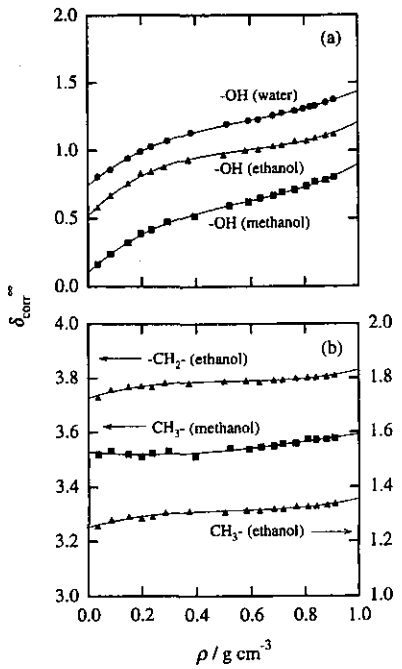

Figure 8. Density dependence of δ^{∞}_{corr} of hydroxyl protons (a) and protons attached to the carbons (b) of water (circles), methanol (squares), and ethanol (triangles) in carbon dioxide at 313.3 K. The lines represent the third-order regressed fits of the data.

view of the nearly invariant δ^{∞}_{corr}. To interpret this characteristic behavior, two practical models (denoted as A and B) are applied. In the former model A, it is considered that the solvation sphere in the gaslike state is being occupied with solvent molecules in proportion to ρ: the radial distribution function is simply replaced by the Boltzmann factor. Once the solvation sphere is completely saturated with solvent molecules, the solvation structure should remain almost unchanged (the intermediate state). The subsequent change in the liquidlike state can be attributed to reconstruction of the solvation structure and/or formation of an outer solvation sphere.[33] The latter model B, on the other hand, is based on Tucker's framework,[32] the original idea of which was put forward by Sun et al.[34] The solvent density inhomogeneity around the solute molecule, usually expressed as the local solvent density enhancement (or depletion), happens particularly in the gaslike and intermediate states and diminishes in the liquidlike state. The near invariance in the intermediate state can be interpreted in terms of the fact that the local solvent density cannot be altered until the bulk solvent density begins to exceed the local solvent density. The two models A and B are conceptually different. Without any further information, however, we cannot elucidate which of the two models is appropriate at this stage. Hence, two types of consideration are given to the characteristic behavior on the basis of the models A and B.

Solvation Structure Based on Model A. In the gaslike state, δ^{∞}_{corr} shows a linear relationship with ρ:

$$\delta^{\infty}_{corr}(\rho) = \delta_0 + \delta_1\rho \quad \text{at} \quad \rho < 0.2 \text{ g cm}^{-3} \tag{9}$$

where the coefficients are recalculated with four data points (Table 2). The model A assumes that the radial distribution function, $g(r)$, in the gaslike state is replaced by the Boltzmann factor. Thus, δ_1 is given by

$$\delta_1 = \frac{\delta^{\infty}_{corr} - \delta_0}{\rho} = -10^6 \sum_i \left\{ \frac{N_A}{M} \int \sigma_i(r) \exp\left(-\frac{u(r)}{kT}\right) 4\pi r^2 \, dr \right\} \tag{10}$$

Here, k is the Boltzmann constant and $u(r)$ is the intermolecular potential. Let us suppose a Lennard-Jones (6−12) potential for $u(r)$. The potential parameters of the collision diameter, σ_{12}, and the depth of potential, ϵ_{12}, between the solute and CO_2 molecules are summarized in Table 3.[35,36] Hereafter, the solutes are divided into two groups in terms of the polarity of the molecule: for nonpolar solutes $\sigma_i(r) \approx \sigma_W(r)$ holds, whereas for polar solutes $\sigma_i(r)$ is expressed as a combination of $\sigma_W(r)$ and $\sigma_e(r)$.

For nonpolar n-hexane and benzene, the solvent-induced chemical shift is mainly caused by van der Waals interaction, $\sigma_W(r)$. According to Bothner-By[37] and Raynes et al.,[27] $\sigma_W(r)$ is proportional to the polarizability, α_2, and the ionization energy, I_2, of the solvent molecule, and inversely proportional to the intermolecular distance, r, to the sixth power:

$$\sigma_W(r) = -B_W \frac{3\alpha_2 I_2}{(4\pi\epsilon_0)^2 r^6} \tag{11}$$

where ϵ_0 is the permittivity of a vacuum and B_W is a constant. Raynes et al.[27] first reported $B_W = 1.1 \times 10^{-27}$ V^{-2} m^2 (=1.0 $\times 10^{-18}$ esu) for protons of hydrocarbons; however, later Trappeniers and Oldenziel[30] pointed out that $|\sigma_W|$ for protons of methane was about 0.7 times that expected with Raynes's B_W. Substituting eq 11 into eq 10 with $\alpha_2 = 2.95 \times 10^{-40}$ F m^2 [38] and $I_2 = 2.21 \times 10^{-18}$ J [39] for CO_2, we obtain $B_W = 0.54 \times 10^{+27}$ V^{-2} m^2 for the CH_3 protons of n-hexane, which is similar to the result of Trappeniers and Oldenziel.[30] Here δ_1 of the CH_2 protons of n-hexane is excluded from subsequent discussion because of the unreliability. The δ_1 of benzene is comparable to those of polar dichloromethane, chloroform, and acetonitrile, leading to a large value of B_W unreasonably. This cannot be rationalized at present, but it might be due to a failure in the Boltzmann factor approximation to $g(r)$ and/or other contribution(s) such as interaction between CO_2 and π-electrons of benzene.[40]

For polar solute molecules (dichloromethane, chloroform, acetonitrile, water, methanol, and ethanol), an additional contribution of $\sigma_e(r)$ must be introduced. In the simplest model of Bunkingham[41] for an axially symmetric approximation of a R−H bond, $\sigma_e(r)$ is proportional to the electric field strength, E_z, along the R−H bond:[42,43]

$$\sigma_e(r) = -A_e E_z(r) \tag{12}$$

where A_e is a constant and dependent on the character of the R−H bond. The electric field, E_z, is produced by the quadrupole moment of CO_2 ($\Theta_2 = -14.3 \times 10^{-40}$ C m^2)[44] and the induced dipole moment arising from the permanent dipole moment, μ_1, of the solute molecule[45] (Table 3). Thus, $\sigma_e(r)$ is[27]

$$\sigma_e(r) = \sigma_{e,quad}(r) + \sigma_{e,ind}(r) = -A_e\{E_{z,quad}(r) + E_{z,ind}(r)\} \tag{13}$$

with

$$E_{z,quad} = -\frac{3\Theta_2}{2(4\pi\epsilon_0)r^4} f_{quad}(\theta_2,\phi_2) \tag{14}$$

and

TABLE 2: Values of δ_0, δ_1, δ_2, and δ_3 for δ^{∞}_{corr} of a Variety of Solutes in Carbon Dioxide at 313.3 K[a]

	$\delta^{\infty}_{corr} = \delta_0 + \delta_1\rho + \delta_2\rho^2 + \delta_3\rho^3$				$\delta^{\infty}_{corr} = \delta_0 + \delta_1\rho$ ($\rho < 0.2$ g cm^{-3})	
solute	δ_0	δ_1/cm^3 g^{-1}	δ_2/cm^6 g^{-2}	δ_3/cm^9 g^{-3}	δ_0	δ_1/cm^3 g^{-1}
n-hexane (−CH_3)	1.00(1)	0.09(8)	−0.16(19)	0.16(13)	1.00(2)	0.07(10)
n-hexane (−CH_2−)	1.42(2)	0.06(10)	−0.17(23)	0.18(16)	1.42(2)	0.04(11)
benzene	7.28(2)	0.42(11)	−0.64(24)	0.40(17)	7.29(2)	0.27(10)
dichloromethane	5.14(1)	0.31(8)	−0.36(19)	0.23(13)	5.15(2)	0.25(9)
chloroform	7.17(3)	0.34(24)	−0.77(56)	0.61(38)	7.17(4)	0.22(24)
acetonitrile	1.69(1)	0.19(8)	−0.25(19)	0.22(13)	1.69(2)	0.17(14)
water	0.71(1)	1.60(9)	−1.91(21)	1.01(14)	0.73(2)	1.18(11)
methanol (−CH_3)	3.50(2)	−0.09(16)	0.24(38)	−0.09(26)	3.50(5)	−0.07(34)
methanol (−OH)	0.07(2)	1.82(17)	−2.39(41)	1.36(28)	0.08(2)	1.41(14)
ethanol (−CH_3)	1.22(2)	0.28(11)	−0.48(25)	0.30(17)	1.23(5)	0.18(37)
ethanol (−CH_2−)	3.69(2)	0.32(11)	−0.57(27)	0.35(18)	3.70(5)	0.26(34)
ethanol (−OH)	0.49(3)	1.97(20)	−2.88(47)	1.60(32)	0.50(4)	1.54(23)

[a] The 95% confidence limit in the least significant digits is given in parentheses.

TABLE 3: Values of $\bar{r}$ Estimated at Given *n* and Related Parameters for a Variety of Solutes in Carbon Dioxide at 313.3 K

solute	σ_{12}[a]/10^{-10} m	$2^{1/6}\sigma_{12}$/10^{-10} m	$\epsilon_{12}k^{-1}$[a]/K	μ_1[b]/10^{-30} C m	A_e/10^{-17} V^{-1} m	$\delta^{\infty}_{corr} - \delta_0$ at $\rho = 0.91$ cm^3 g^{-1}	$\bar{r}$/10^{-10} m, n=6	$\bar{r}$/10^{-10} m, n=12
n-hexane (−CH_3)	4.95	5.56	280	0		0.07	4.4	4.9
dichloromethane	4.38	4.91	278	5.34	1.4	0.15	4.2	4.8
chloroform	4.71	5.29	249	3.47	1.5	0.12	4.4	5.0
acetonitrile	4.01[c]	4.50	276[c]	13.1	0.35	0.12	4.1	4.6
water	3.32[c]	3.73	269[c]	6.18	6.93	0.61	3.8	4.4
methanol (−OH)	3.79	4.25	310	5.67	9.94	0.69	3.9	4.5
ethanol (−OH)	4.23	4.74	273	5.64	13.3	0.60	4.2	5.0

[a] Obtained from the literature[36] by using $\sigma_{12} = (1/2)(\sigma_1 + \sigma_2)$ and $\epsilon_{12} = (\epsilon_1\epsilon_2)^{1/2}$. [b] Cited from ref 45. [c] Evaluated by assuming that σ_1 and ϵ_1 in a Lennard-Jones (6−12) potential were the same as the corresponding values in a Stockmeyer potential.[35]

$$E_{z,ind} = \frac{\mu_1\alpha_2}{(4\pi\epsilon_0)^2 r^6} f_{ind}(\theta_1) \qquad (15)$$

where f_{quad} and f_{ind} are the functions of orientational angles of the solvent quadrupole (θ_2, ϕ_2) and the solute dipole (θ_1), respectively. The contributions of $\sigma_W(r)$, $\sigma_{e,quad}(r)$, and $\sigma_{e,ind}(r)$ are separately calculated as a function of r in Figure 9: the calculations are made by assuming $f_{quad}(\theta_2,\phi_2) = f_{ind}(\theta_1) = 1$ for $\mu_1 = 5 \times 10^{-30}$ C m (solid line) and 1.5×10^{-29} C m (broken line) with $A_e = 1.5 \times 10^{-17}$ V^{-1} m and $B_W = 0.54 \times 10^{-27}$ V^{-2} m^2, which are appropriately optimized for the C−H_n protons as mentioned later. As shown in Figure 9, $\sigma_{e,ind}(r)$ is much smaller than $\sigma_W(r)$ and $\sigma_{e,quad}(r)$ even for $\mu_1 = 1.5 \times 10^{-29}$ C m (broken line).

To relate $\sigma_e(r)$ with r, the parameter A_e has to be determined for each polar solute. We proceed on the basis of the two assumptions that the B_w determined for the CH_3 protons of *n*-hexane remains unchanged for the protons of polar molecules and $f_{quad}(\theta_2,\phi_2)$ and $f_{ind}(\theta_1)$ are fixed to be unity. The former assumption may be reasonable in view of the previous work[27] for hydrogen chloride: A_e is 20 times that of a C−H bond, whereas B_w is similar to that of a C−H bond. The latter assumption may not be valid, but the obtained A_e probably relates $\sigma_e(r)$ with r at an arbitrarily fixed orientation in a one-dimensional map. The values of A_e thus obtained from δ_1 are presented in Table 3. Here we exclude the data of the CH_3 and CH_2 protons of methanol and ethanol because their shielding constants could be affected by a change in the hydroxyl group.

With the values of A_e and B_W, the solvation structure around the solute molecule in CO_2 ($\rho = 0.91$ g cm^{-3}) is tentatively estimated on the basis of the cage model[11,16] that *n* solvent molecules at the average distance, $\bar{r}$, in the solvation sphere mainly contribute to σ:

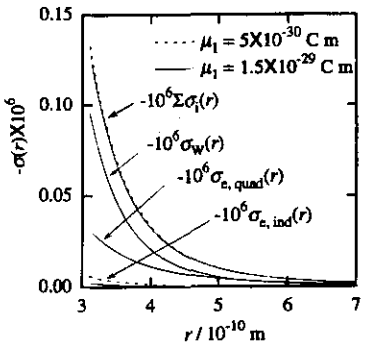

Figure 9. Calculated contributions of $\sigma_W(r)$, $\sigma_{e,quad}(r)$, and $\sigma_{e,ind}(r)$ for C−H_n protons of polar solutes as a function of r. Values of $A_e = 1.5 \times 10^{-17}$ V^{-1} m and $B_W = 0.54 \times 10^{-27}$ V^{-2} m^2 are used for the calculations, and $f_{quad}(\theta_2,\phi_2) = f_{ind}(\theta_1) = 1$ is assumed.

$$\delta^{\infty}_{corr} - \delta_0 = -10^6 \sum_i \langle\sigma_i\rangle = -10^6 \sum_i \{n\sigma_i(\bar{r})\}$$

$$= -10^6 n\left[-B_W\frac{3\alpha_2 I_2}{(4\pi\epsilon_0)^2\bar{r}^6} - A_e\left[-\frac{3\Theta_2}{2(4\pi\epsilon_0)\bar{r}^4} + \frac{\mu_1\alpha_2}{(4\pi\epsilon_0)^2\bar{r}^5}\right]\right] \qquad (16)$$

The experimental values of $(\delta^{\infty}_{corr} - \delta_0)$ at $\rho = 0.91$ g cm^{-3} are given in the seventh column of Table 3. The $(\delta^{\infty}_{corr} - \delta_0)$ can determine the average distance, $\bar{r}$, if *n* is given. The $\bar{r}$ values are listed in Table 3 at $n = 6$ and 12, together with the distance at the minimum of the Lennard-Jones potential, $2^{1/6}\sigma_{12}$. Note that our estimation is based on simple approximations: the protons are situated at the periphery of the molecule, whereas interactions are treated between the centers of two molecules, and the proton shielding constant in the molecule is dealt with separately by neglecting contributions from other parts of the

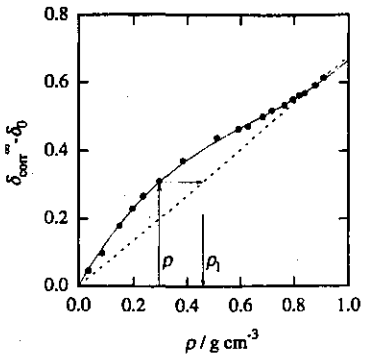

Figure 10. A representative plot for estimation of the local solvent density around water in carbon dioxide at 313.3 K. The solid line represents the third-order regressed fit of the data and the broken line the linearly regressed fit of the data at 0.8 g cm^{-3} < ρ through the origin.

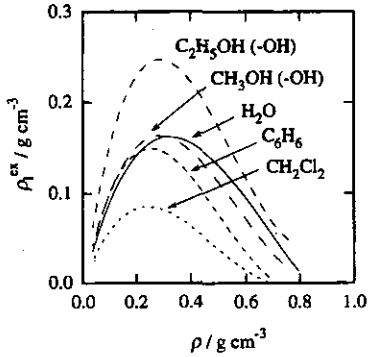

Figure 11. Bulk density dependence of ρ_l^{ex} around various solute molecules in carbon dioxide at 313.3 K.

molecule, although it should be considered in terms of the gross properties of the molecule. The parameters A_e and B_W will involve such uncertainties, which might compensate the average distance. If the Boltzmann factor approximation to $g(r)$ in the gaslike state is correct, the resultant average distance, $\bar{r}$, could be a measure of the solvation structure around the solute molecule.

Local Solvent Density Enhancement Based on Model B. In accordance with the previous treatment,[32] the excess local density, ρ_l^{ex}, of solvent in the solvation sphere is defined as

$$\rho_l^{ex} = \rho_l - \rho \tag{17}$$

where ρ_l is the local solvent density in the solvation sphere. In this model ρ_l approaches ρ in the liquidlike state; hence, it is reasonably considered that $g(r)$ in eq 7 should be invariable with ρ. This hypothesis straightforwardly leads to a linear relationship between $\delta_{corr}^{\infty} - \delta_0$ and ρ at higher densities unless the average orientations of solvent molecules are strongly dependent on ρ. Thus, the reference line can be obtained by making a linearly regressed fit of the data in the range of 0.8 g cm^{-3} < ρ through the origin. The local solvent density at each ρ value can then be extracted by comparing the measured value to the reference one. This is a very convenient procedure because it does not require explicit expressions for $\sigma_i(r)$. A representative plot is shown in Figure 10.

One can know that $\partial\delta_{corr}^{\infty}/\partial\rho$ at ρ < 0.2 g cm^{-3} is much larger than the corresponding value at 0.8 g cm^{-3} < ρ in most of the solutes except for *n*-hexane and acetonitrile. This difference reflects the degree of attractive interaction between the solute and CO_2 molecules. From this viewpoint the solutes may be classified into two groups: in one group the local solvent density around the attractive solute is appreciably enhanced in the gaslike and intermediate states, whereas in another group the local solvent density around the weakly attractive solute is enhanced a little or not.[46] For *n*-hexane and acetonitrile the uncertainties of the data prevent us from extraction of small ρ_l^{ex}; however, this fact suggests a very weak interaction between the methyl group and CO_2 molecules.

The value of ρ_l^{ex} is plotted against ρ in Figure 11. The ρ_l^{ex} for chloroform is eliminated because the data points are scattered. As seen from Figure 11, ρ_l^{ex} increases rapidly and reaches a maximum at ρ = 0.2–0.4 g cm^{-3}, and then decreases with increasing ρ. This observation seems to be reasonable in comparison with the previous results of various spectroscopic shifts.[32] In fact, Wada et al.[47] reported that the excess local density about a benzene molecule in CO_2 at 318.2 K has a maximum value of 0.21 g cm^{-3} at $\rho \approx$ 0.25 g cm^{-3}. The maximum value of ρ_l^{ex} = 0.15 g cm^{-3} for benzene in this study is slightly small, but its position is in good agreement with Wada's result.[47] The analytical procedure developed on the basis of model B is very practical, and the solvent-induced chemical shift can provide a feasible picture of ρ_l^{ex}.

Conclusion

A newly designed high-pressure NMR flow cell withstanding pressures above 30 MPa has been established. The ^{1}H chemical shifts of a variety of simple solutes in gaseous and supercritical carbon dioxide have been measured in the wide pressure range between 2 and 30 MPa at 313.3 K. The chemical shifts of hydroxyl protons of water, methanol, and ethanol in carbon dioxide at 20.0 MPa showed a high-frequency shift due to intermolecular hydrogen bonding with increasing concentration. Compared with the corresponding values in carbon tetrachloride, the existence of a specific interaction between alcohol and carbon dioxide molecules was demonstrated, which is in agreement with the previous results of FT-IR spectroscopy by Fulton et al.[4] The density dependence of the susceptibility-corrected chemical shift at infinite dilution was well expressed as the polynomial equation of the third power of density. In view of the observed density dependence, we proposed that a variation of solvation structure should be deliberated in terms of three distinct density regions, i.e., gaslike, intermediate, and liquidlike. In the gaslike and liquidlike states the solvation structure rapidly varies with increasing bulk density, and in the intermediate state the solvation structure remains almost unchanged although the bulk density changes drastically. The solvent-induced chemical shift was discussed on the basis of two different models. Temperature-variable chemical shift measurements will elucidate which of the two is adequate for describing a change in the solvation structure with the solvent density. The precise measurements of NMR chemical shifts, as presented here, can provide promising results for understanding the surroundings of solute molecules in supercritical fluids.

Acknowledgment. M.K. is much indebted to Dr. K. Torii and Dr. C. C. Liew for their continuous encouragement and helpful discussion. M.K. gratefully acknowledges Dr. T. Yokoyama for sharing the NMR instrument, and also thanks Mr. S. Sasaki, Mr. K. Mori, Mr. M. Yoneya, and Mr. S. Ito for their kind assistance.

References and Notes

(1) For example, Randolph, T. W.; Clark, D. S.; Blanch, H. W.; Prausnitz, J. M. *Science* **1988**, *239*, 387. Ikushima, Y.; Saito, N.; Arai, M.;

Blanch, H. W. *J. Phys. Chem.* **1995**, *99*, 8941. Nakamura, K. *TIBTECH* **1990**, *8*, 288. Ikushima, Y. *Adv. Colloid Interface Sci.* **1997**, *71/72*, 259.

(2) Angus, S.; Armstrong, B.; de Reuck, K. M. *International Thermodynamic Table of the Fluid State-3 Carbon Dioxide*; IUPAC; Blackwell Science: Oxford, 1976.

(3) For example, Yonker, C. R.; Smith, R. D. *J. Phys. Chem.* **1988**, *92*, 2374. Akimoto, S.; Kajimoto, O. *Chem. Phys. Lett.* **1993**, *209*, 263. Ikushima, Y.; Saito, N.; Arai, M. *J. Phys. Chem.* **1992**, *96*, 2293. Meredith, J. C.; Johnston, K. P.; Seminario, J. M.; Kazarian, S. G.; Eckert, C. A. *J. Phys. Chem.* **1996**, *100*, 10837.

(4) Fulton, J. L.; Yee, G. G.; Smith, R. D. *J. Am. Chem. Soc.* **1991**, *113*, 8327.

(5) For example, Hertz, H. G. In *Water: A Comprehensive Treatise*; Franks, F., Ed.; Plenum: New York, 1973; Vol. 3, Chapter 7. Grant, D. M.; Mayne, C. L.; Liu, F.; Xiang, T. X. *Chem. Rev.* **1991**, *91*, 1591. Kanakubo, M.; Ikeuchi, H.; Satô, G. P.; Yokoyama, H. *J. Phys. Chem. B* **1997**, *101*, 3827. Kanakubo, M.; Uda, T.; Ikeuchi, H.; Satô, G. P. *J. Solution Chem.* **1998**, *27*, 645. Kanakubo, M.; Ikeuchi, H.; Satô, G. P. *J. Chem. Soc., Fraday Trans.* **1998**, *94*, 3237.

(6) Yonker, C. R.; Wallen, S. L.; Linehan, J. C. *J. Supercrit. Fluids* **1995**, *8*, 250.

(7) Linehan, J. C.; Wallen, S. L.; Yonker, C. R.; Bitterwolf, T. E.; Bays, J. T. *J. Am. Chem. Soc.* **1997**, *119*, 10170.

(8) Dardin, A.; Cain, J. B.; DeSimone, J. M.; Johnson, C. S., Jr.; Samulski, E. T. *Macromolecules* **1997**, *30*, 3593.

(9) Dardin, A.; DeSimone, J. M.; Samulski, E. T. *J. Phys. Chem. B* **1998**, *102*, 1775.

(10) Vanni, H.; Earl, W. L.; Merbach, A. E. *J. Magn. Reson.* **1978**, *29*, 11.

(11) Lim, Y.; Nugara, N. E.; King, A. D., Jr. *J. Phys. Chem.* **1993**, *97*, 8816.

(12) Pfund, D. M.; Zemanian, T. S.; Linehan, J. C.; Fulton, J. L.; Yonker, C. R. *J. Phys. Chem.* **1994**, *98*, 11846.

(13) For example, Jessop, P. G.; Ikariya, T.; Noyori, R. *Science* **1995**, *269*, 1065. Jessop, P. G.; Ikariya, T.; Noyori, R. *Chem. Rev.* **1999**, *99*, 475.

(14) Lamb, D. M.; Barbara, T. M.; Jonas, J. *J. Phys. Chem.* **1986**, *90*, 4210.

(15) Aizawa, T.; Sato, O.; Ikushima, Y.; Hatakeda, K.; Saito, N. *Rev. High-Pressure Sci. Technol.* **1998**, *7*, 1426.

(16) Rummens, F. H. A.; Raynes, W. T.; Bernstein, H. J. *J. Phys. Chem.* **1968**, *72*, 2111.

(17) Momoki, K.; Fukazawa Y. *Anal. Sci.* **1991**, *7*, 403.

(18) Dickinson, W. C. *Phys. Rev.* **1951**, *81*, 717.

(19) Becker, E. D. *High-Resolution NMR Theory and Chemical Applications*, 2nd ed.; Academic: New York, 1980; Chapter 4.

(20) Buckingham, A. D.; Schaefer, T.; Schneider, W. G. *J. Chem. Phys.* **1960**, *32*, 1227.

(21) Landolt, H. A.; Börnstein, R. *Zahlenwerte und Functionen*, 6th ed.; Springer-Verlag: Berlin, 1967; Vol. II, Part 10.

(22) Symons, M. C. R. *Chem. Soc. Rev.* **1983**, *12*, 1.

(23) Karachewski, A. M.; Howell, W. J.; Eckert, C. A. *AIChE J.* **1991**, *37*, 65.

(24) Wendt, M. A.; Meiler, J.; Weinhold, F.; Farrar, T. C. *Mol. Phys.* **1998**, *93*, 145.

(25) Gutowsky, H. S.; Saika, A. *J. Chem. Phys.* **1953**, *21*, 1688.

(26) Hoffmann, M. M.; Conradi, M. S. *J. Am. Chem. Soc.* **1997**, *119*, 3811. Hoffmann, M. M.; Conradi, M. S. *J. Phys. Chem. B* **1998**, *102*, 263.

(27) Raynes, W. T.; Buckingham, A. D.; Bernstein, H. J. *J. Chem. Phys.* **1962**, *36*, 3481.

(28) Buckingham, A. D.; Pople, J. A. *Discuss. Faraday Soc.* **1956**, *22*, 17.

(29) C. J. Jameson, *Chem. Rev.* **1991**, *91*, 1375.

(30) Trappeniers, N. J.; Oldenziel, J. G. *Physica* **1976**, *82A*, 581.

(31) The bulk magnetic susceptibility contribution has been subtracted in the present paper.

(32) Tucker, S. C. *Chem. Rev.* **1999**, *99*, 391 and references cited therein.

(33) It is practically impossible to separate the two contributions rigorously; however, the structural change in the first solvation sphere will be of primary importance in view of the distance sensitivity of δ^{∞}_{conf}.

(34) Sun, Y.; Fox, M. A.; Johnston, K. P. *J. Am. Chem. Soc.* **1992**, *114*, 1187.

(35) Values of σ_{12} and ϵ_{12} were calculated on the basis of the empirical combining laws: $\sigma_{12} = (1/2)(\sigma_1 + \sigma_2)$ and $\epsilon_{12} = (\epsilon_1\epsilon_2)^{1/2}$, where σ_i and ϵ_i ($i = 1$ and 2) are the collision diameters and the depths of potential between the solute molecules ($i = 1$) and between the solvent molecules ($i = 2$), respectively. For lack of data for acetonitrile and water, σ_1 and ϵ_1 in a Lennard-Jones (6−12) potential were assumed to be the same as the corresponding values in a Stockmeyer potential. All the data were taken from ref 36.

(36) Hirschfelder, J. O.; Curtiss, C. F.; Bird, R. B. *Molecular Theory of Gases and Liquids*; John Wiley & Sons: New York, 1964; Appendix.

(37) Bothner-By, A. A. *J. Mol. Spectrosc.* **1960**, *5*, 52.

(38) Landolt, H. H.; Börnstein, R. *Zahlenwerte und Functionen*, 6th ed.; Springer-Verlag: Berlin, 1951; Vol. I, Part 3.

(39) Field, F. H.; Franklin, J. L. *Electron Impact Phenomena*; Academic: New York, 1970.

(40) A benzene molecule is surely quadrupolar as is an acetylene molecule; however, we expect that the polar effect, i.e., the quadrupole−quadrupole interaction, will make less contribution to δ_1. The quadrupolar effect on the shielding constant of acetylene was discussed in ref 41.

(41) Buckingham, A. D. *Can. J. Chem.* **1960**, *38*, 300.

(42) In the original paper (ref 41), σ_e also depends on the square electric field. However, the E_z term is normally dominant in σ_e for protons.

(43) Equation 12 refers only to the uniform electric field. The electric field gradient may contribute to σ_e to a lesser extent.

(44) Graham, C.; Imrie, D. A.; Raab, R. E. *Mol. Phys.* **1998**, *93*, 49.

(45) Lide, D. R., Frederikse, H. P. R., Eds. *Handbook of Chemistry and Physics*, 78th ed.; CRC: New York, 1997; Chapter 9.

(46) The "attractive" and "weakly attractive" solutes are rigorously defined in terms of the solute−solvent correlation function integral. See ref 32.

(47) Wada, N.; Saito, M.; Kitada, D.; Smith, R. L., Jr.; Inomata, H.; Arai, K.; Saito, S. *J. Phys. Chem. B* **1997**, *101*, 10918.